JOURNAL OF SPACECRAFT AND ROCKETS
Vol. 38, No. 2, March–April 2001

Semiempirical Prediction of Pitch Damping Moments for Configurations with Flares

F. G. Moore*
Aeroprediction, Inc., King George, Virginia 22485
and
T. C. Hymer†
U.S. Naval Surface Warfare Center, Dahlgren, Virginia 22448

New capability has been added to the Naval Surface Warfare Center aeroprediction code to allow aerodynamics to be predicted for Mach numbers up to 20 for configurations with flares. This new capability includes extending the static aerodynamic predictions for Mach numbers less than 1.2, improving the body alone pitch damping for Mach numbers above 2.0, and developing a new capability for pitch damping of flared configurations at Mach numbers up to 20. This new capability for flared configurations was validated for several different configurations in the Mach number range of 2–8.8. Whereas flared configuration aerodynamics have been validated only up to Mach 8.8, static aerodynamics have been validated in previous references for other configurations as high as Mach number 14. Most validations of the aeroprediction code have been performed between Mach numbers of 0.1 and 5, where most experimental data are available. In general, pitch damping predictions of the improved capability were within 20% of either experimental data or computational fluid dynamics calculations. This accuracy level is believed to be quite adequate for dynamic derivatives in the preliminary design stage. These new additions to the aeroprediction code will be transitioned to users as part of the 2002 version of the code (AP02).

Nomenclature

A_B	=	base area, $\pi d_B^2/4$
A_{REF}	=	reference area (maximum cross-sectional area of body, if a body is present, or planform area of wing, if wing alone), ft^2
C_A	=	axial force coefficient
$C_{A_B}, C_{A_f}, C_{A_W}$	=	base, skin-friction, and wave components, respectively, of axial force coefficient
C_{A_F}	=	forebody axial force coefficient ($C_{A_F} = C_{A_f} + C_{A_W}$)
C_D	=	drag coefficient
C_L	=	lift coefficient
C_M	=	pitching moment coefficient (based on reference area and body diameter, if body present, or mean aerodynamic chord, if wing alone)
$C_{M_q} + C_{M_{\dot\alpha}}$	=	pitch damping moment coefficient $[C_M(q)/(qd/2V_\infty) + C_M(\dot\alpha)/(\dot\alpha d/2V_\infty)]$
C_{M_α}	=	pitching moment coefficient derivative, 1/rad
$C_M(q)$	=	pitching moment coefficient due to a constant pitching rate of q
$C_M(\dot\alpha)$	=	pitching moment coefficient due to a constant vertical acceleration of $\dot\alpha$
C_N	=	normal force coefficient
C_{N_α}	=	normal force coefficient derivative, 1/rad
d_B	=	body diameter at base, ft
d_r	=	reference body diameter, ft
$\ell, \ell_n, \ell_a, \ell_f$	=	body length, nose length, afterbody length, and flare length, respectively
ℓ_1	=	distance from cone apex to flare–cylinder juncture
M_∞	=	freestream Mach number
N	=	normal force, lb
R_N	=	Reynolds number
r	=	local body radius, ft
V_∞	=	freestream velocity, ft/s
x, y, z	=	axis system fixed with x along centerline of body
$x_{\text{c.p.}}, \bar{x}_{\text{c.p.}}$	=	center of pressure (in feet or calibers, respectively, from some reference point that can be specified) in x direction
α	=	angle of attack, deg
θ_f	=	flare angle, deg
Φ	=	roll position of missile fins [$\Phi = 0$ deg corresponds to fins in the plus (+) orientation, $\Phi = 45$ deg corresponds to fins rolled to the cross (×) orientation]

Subscripts

C	=	cone
c.g.	=	center of gravity
f	=	flare

Introduction

THE 1998 version of the Naval Surface Warfare Center, Dahlgren Division (NSWCDD) aeroprediction code (AP98)[1] is the most complete and comprehensive semiempirical weapon aerodynamics code produced to date. It includes the capability to predict planar aerodynamics in the roll positions of $\Phi = 0$ deg (fins in + or plus orientation as viewed from the rear of the missile) and $\Phi = 45$ deg (fins in × or cross roll orientation as viewed from the rear of the missile) over a broad range of flight conditions and configuration geometries with good average accuracy, computational times, and ease of use. Flight conditions include angles of attack (AOA) up to 90 deg, control deflections of up to ±30 deg, and Mach numbers up to 20. In addition, the second-order shock expansion method was extended to include real gas effects for Mach numbers greater than 6 to provide engineering estimates of convective heat transfer. Also, the local loads were distributed over the body and lifting surfaces to aid the structural engineer in performing preliminary structural analysis. All of the technology utilized in the AP98 has been recently published in a new book[2] by one of the present authors. Configuration geometries include axisymmetric and nonaxisymmetric body shapes with sharp, blunt, or truncated nose tips, with or without a

Received 23 March 2000; revision received 19 October 2000; accepted for publication 3 November 2000; presented as Paper 2001-0101 at the AIAA 39th Aerospace Sciences Meeting, Reno, NV, 8–11 January 2001.

*President, 9449 Grover Drive, Suite 201. Associate Fellow AIAA.
†Aerospace Engineer, Systems Engineering Branch, Weapons Systems Department, Dahlgren Division.

Table 1 AP98[1] methods for dynamic derivatives

Property	Component/Mach number region: Subsonic $M < 0.8$	Transonic $0.8 \le M \le 1.2$	Low supersonic $1.2 < M \le 1.8$	Mod/high supersonic $1.8 < M \le 6.0$	Hypersonic $M > 6.0$
Body alone	Empirical	Empirical	Empirical	Empirical	Empirical
Wing and interference roll damping moment	Lifting surface theory	Empirical	Linear thin wing theory	Linear thin wing theory	Linear thin wing theory
Wing Magnus moment	Assumed zero	Assumed zero	Assumed zero	Assumed zero	Assumed zero
Wing and interference pitch damping moment	Lifting surface theory	Empirical	Linear thin wing theory	Linear thin wing theory	Linear thin wing theory

boattail or flare. Up to two sets of planar or cruciform fins are allowed. New technology has recently been developed[3] to allow both six- and eight-fin options in the fin considerations as well. Also, many of the constants used in the aeroprediction code have been refined[4] based on a more recent wind-tunnel database, allowing more accurate aerodynamic estimates at AOA. Average accuracies are ±10% for normal and axial force and ±4% of body length for center of pressure. Average accuracy means that enough AOA or Mach numbers are considered to get a good statistical sample. On occasion, a single data point can exceed these average accuracy values. Ease of use has been significantly enhanced over older versions of the aeroprediction code (APC) through a personal computer-based pre- and postprocessor package.[5] This package has allowed inputs for configuration geometries to be simplified significantly by many automated nose shape options.

The code has been made operational up to Mach 20, which is above the upper Mach boundary of where weapons fly. However, the code has been validated fairly extensively up to Mach 4.63 and somewhat less extensively to Mach 14 (Ref. 1). Dynamic derivatives have been validated only to Mach numbers as high as 8.8 (Ref. 6). Although the code has been validated extensively only to Mach numbers of about 5, the authors feel fairly comfortable that the aerodynamics can be computed to Mach 20. There are several reasons for this confidence in high-Mach-number computations. First, theoretical methods are used for the low AOA methods and real gas effects have been accounted for at Mach numbers greater than 6. These real gas effects only show small effects on forces and moments but very large effects on local temperatures and aerodynamic heating. Second, wing alone, body alone, wing–body interference effects, base drag, and other nonlinearities tend toward an asymptote as Mach number increases. This asymptotic effect is attributed in part to the Newtonian flow mechanism, where at high Mach number the momentum of the air particles is lost almost entirely on direct impact of a surface, as opposed to wrapping around the surface and carrying some of the momentum with it as at lower Mach numbers. Thus, although the flow is highly nonlinear at high Mach numbers, the methods used in the AP98[1] have given acceptable accuracy for the Mach numbers where data have been found. As more high Mach number data become available, additional validation and refinement of the code can take place.

Although the AP98 is a very powerful tool, several limitations and areas of improvement still remain. Most of these needs are driven by the desire of future weapon designers to perform trade studies on new and innovative concepts that may fall outside of the current capability of the AP98. An example of this type of requirement is the multifin requirement that has just been completed.[3] Another example of this type of requirement is to include the capability to deflect the rear segment of a fin (sometimes referred to as flaperon or aileron) for control, as opposed to the entire fin. Also, the capability to predict drag accurately for all power on conditions is desired. Finally, improvement in aerodynamics of projectiles that use a flare for stability (as opposed to fins) is needed. This paper will deal with the last problem area of improving aerodynamics of configurations that use a flare for stability. Figure 1 illustrates the typical geometrical parameters associated with a flare. The two most important parameters are the flare length and angle, which can also be expressed in terms of the flare base to forward or reference diameter.

The problem of inaccurate aerodynamic predictions for flared configurations from the APC first came to the authors' attention a couple of years ago in the form of the pitch damping moment

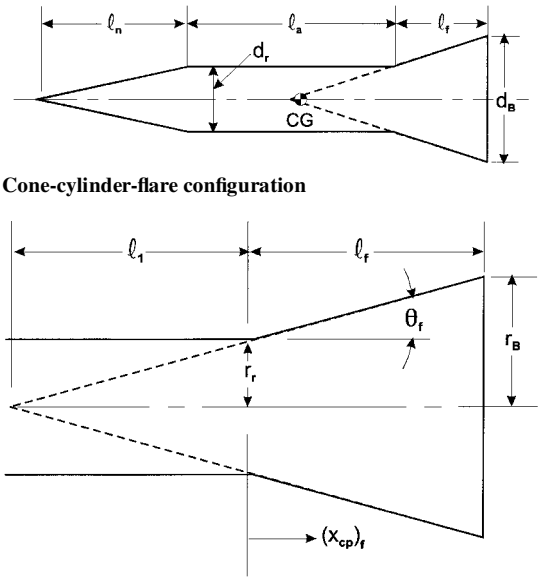

Fig. 1 Typical flare configuration with the significant geometrical parameters.

coefficient predictions for a flared projectile concept at an AIAA meeting. The increased interest in the use of flares for stability in recent years, particularly for higher Mach numbers (see Refs. 7–9, for example), has also led the authors to feel that improvements in the aerodynamic predictions of flared projectiles were needed.

As a result of the increased interest in flared projectiles for higher Mach number applications, the authors decided to take another look at the APC to determine its weak areas with respect to flared shaped projectiles. Several problem areas were identified. First, for the static aerodynamics, no particular attention was given for flared projectiles for $M_\infty < 1.2$. For $M_\infty \ge 1.2$, low AOA aerodynamics are computed by theoretical methods such as second-order Van Dyke or second-order shock expansion theory, and reasonable estimates of static aerodynamics (C_A, C_N, and $x_{c.p.}$) can be obtained from the APC. For $M_\infty < 1.2$, the capability to compute static aerodynamics needs to be incorporated into the code.

The second problem uncovered in the APC prediction of aerodynamics was for the dynamic derivative, $C_{M_q} + C_{M_{\dot\alpha}}$, or pitch damping moment coefficient. Table 1 shows the methods in current use in the AP98 for computing aerodynamic derivatives in general and pitch damping in particular. Although not specifically shown in Table 1, no capability exists at any Mach number in the APC for pitch damping moment of flared projectile shapes. Based on recent computational fluid dynamic (CFD) calculations of projectiles without a flare,[10,11] it was found that the pitch damping moment of configurations without flares needed improvement as well. Table 2 summarizes the weak areas in predicting aerodynamics of flared projectile shapes using the AP98 as problems 1–3.

Analysis

Each of the three weak areas mentioned in the Introduction and listed in Table 2 will be discussed individually in this section of the paper. The discussion will be in terms of modifications that will be made to the AP98 to allow more accurate computations of the

Table 2 AP98 weak areas in predicting aerodynamics of flared configurations

Problem no.	Weak area
1	C_A, C_N, $x_{c.p.}$ not available for $M_\infty < 1.2$ for flare
2	Body alone $C_{M_q} + C_{M_{\dot\alpha}}$ needs improvement for $M_\infty \geq 1.2$ (no flare)
3	No pitch damping contribution for flare in AP98 at any M_∞

aerodynamics of flared projectiles. These modifications will then be a part of the next release of the APC, which will be the AP02 in 2002. More details of the work described in this paper can be found in Ref. 6.

Static Aerodynamics of Flared Projectiles

The wave component of axial force for configurations with small flare angles ($\theta_f < 15$ deg) can be calculated approximately with the perturbation theory of Wu and Aoyoma[12] that was designed for boattails, except that the angle is reversed in sign. There was a sign error in the AP98, but when this error was corrected, approximate estimates of wave drag for $M_\infty < 1.2$ could be computed from the Ref. 12 method. For $M_\infty < 0.9$, the wave drag component is assumed to be zero. Base drag and skin-friction drag were already being computed within the accuracy desired using the AP98, and so no changes in the methodology for these aerodynamic terms were made. As already mentioned, the desired average accuracy on static aerodynamics is ±10% for C_A and C_N and ±4% of body length for center of pressure.

The normal force and pitching moment coefficients and center of pressure for the flares are not predicted at all for $M_\infty < 1.2$. Furthermore, numerical methods do not exist in the AP98 to allow calculations of C_N, C_M, and $x_{c.p.}$ for $M_\infty < 1.2$. Numerical calculations are included for wave drag and normal force coefficient derivatives at low AOA in the transonic regime for body alone cases without flares. However, these calculations are included in a table look-up form to decrease computational time and storage. Also, as will be discussed later in the pitch damping computations for flares, C_N, C_M, and $x_{c.p.}$ for a flare will be needed at all Mach numbers.

To compute $(C_{N_\alpha})_f$ and $(x_{c.p.})_f$, several options are available. The first is to utilize the available values in the APC. Unfortunately, these values are only available for $M_\infty \geq 1.2$, where pressures are computed and integrated over the body surface. Also, the logic of the APC is such that this would require considerable changes to allow these calculations to be performed and brought forward into another subroutine. The second option would be to exercise the APC twice, once with a flare and once without, and subtract the C_{N_α} and C_{M_α} to obtain the flare normal force coefficient derivative and its center of pressure. Again, this is not a very desirable alternative because the APC must be exercised twice to get a single number. A third option, which appears more attractive, is to exercise the APC code offline, compute values of $(C_{N_\alpha})_f$ and $(x_{c.p.})_f$ for $M_\infty \geq 1.2$, and store these in a table look-up as a function of geometric and freestream parameters. For $M_\infty < 1.2$, slender body theory (SBT) can be used to approximate values of $(C_{N_\alpha})_f$ and $(x_{c.p.})_f$. The fourth and most attractive option is to use available cone tables[13] or approximate conical formulas to compute $(C_{N_\alpha})_f$, to use SBT to approximate the center of pressure of the flare and $(C_{N_\alpha})_f$ for $M_\infty < 1.2$, and to include these parameters in a table look-up as a function of geometry and Mach number. This last option can be used because we are assuming the flare is a conical frustrum or can be approximated by a conical frustrum. The last option is the one that will be used in this analysis because it has the advantage of being at least as accurate as current computations in the APC due to use of an exact cone solution from Ref. 13. Also, this approach offers the opportunity to obtain results in a straightforward and direct way from the APC as opposed to more costly approaches of logic change in the APC or cycling through the APC twice to obtain results for the flare alone.

The main negative aspect to this approach is that there will be some slight inconsistency between the normal force coefficient of the flare used for pitch damping calculations and that computed in the AP98 that is used for structural loads and static aerodynamics. However, it is believed the positive aspects of this approach outweigh this minor inconsistency.

The C_{N_α} results for the total cone of Ref. 13 must be corrected to include only the frustrum portion of the cone and also put in the appropriate reference area format. With reference to Fig. 1, the percent of conical shape that is a flare is

$$\frac{A_f}{A_C} = \frac{\pi\left[r_B^2 - r_r^2\right]}{\pi r_B^2} = 1 - \left(\frac{r_r}{r_B}\right)^2 \tag{1}$$

Now the value of C_{N_α} obtained from Ref. 13 is based on the cone base area. Hence, Eq. (1) must be multiplied by A_B/A_r to place it in the same reference area as other C_{N_α} components for the total configuration of Fig. 1. Thus, to relate the value of the C_{N_α} from Ref. 13 for a cone of given angle at a given Mach number to that of a flare, we have

$$\left(C_{N_\alpha}\right)_f = \left(C_{N_\alpha}\right)_C\left[1 - (r_r/r_B)^2\right](r_B/r_r)^2$$

or

$$\left(C_{N_\alpha}\right)_f = \left(C_{N_\alpha}\right)_C\left[(r_B/r_r)^2 - 1\right] \tag{2}$$

Equation (2) is valid at all Mach numbers and for all geometries. However, $(C_{N_\alpha})_C$ is available from Ref. 13 for conditions where the flow is supersonic and the shock wave is attached to the conical tip. For conditions where these two assumptions are not met, SBT will be assumed in conjunction with interpolation. SBT gives

$$\left(C_{N_\alpha}\right)_C = 2.0 \tag{3}$$

This value of $(C_{N_\alpha})_C$ will be assumed for $M_\infty \leq 0.8$. The value of $(C_{N_\alpha})_C$ from Ref. 13 can be used for low AOA calculations of most reasonable flares down to M_∞ of about 1.2. Linear interpolation between SBT and Ref. 13 will be used for $0.8 < M_\infty < 1.2$.

In examining Eq. (2), it is seen that the C_{N_α} for a flare can get quite large if the flare is long or if the flare is short but has a large flare angle. This is why use of a flare is quite popular at higher Mach numbers, where the C_{N_α} for a fin decreases substantially with Mach number increase. The SBT center of pressure for a cone is the same as that from exact theory. The center of pressure is at $\frac{2}{3}$ of the cone length. However, for a conical frustrum, the center of pressure in general will vary between $0.5\ell_f$ and $\frac{2}{3}\ell_f$, depending on the flare angle. For flare angles approaching 0, the value of $(x_{c.p.})_f$ approaches $0.5\ell_f$, whereas for large flare angles, $(x_{c.p.})_f$ approaches $\frac{2}{3}\ell_f$. With reference to Fig. 1, the center of pressure of the flare using SBT can be shown to be[6]

$$(\bar{x}_{c.p.})_f = \frac{2}{3}\left(\frac{1}{1 - r_r/r_B}\right)\left[\frac{1 - (r_r/r_B)^3}{1 - (r_r/r_B)^2}\right] - \frac{r_r/r_B}{1 - r_r/r_B} \tag{4}$$

Results of Eq. (4) are computed and plotted in Fig. 2 as a function solely of the parameter r_r/r_B. As seen in Fig. 2, when the body consists of a cone ($r_r = 0$), then the center of pressure is at $\frac{2}{3}$ of the cone or flare length (which are one and the same). On the other hand,

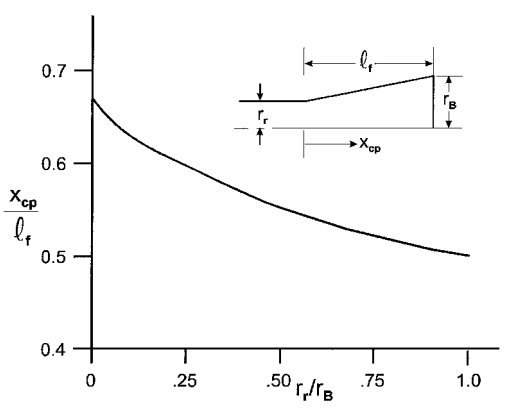

Fig. 2 Slender body theory center of pressure of flare.

when the flare angle goes to zero so that $r_r/r_B = 1.0$, the c.p. goes to $x_{\text{c.p.}}/\ell_f = 0.5$. For most typical flare lengths and angles, $x_{\text{c.p.}}/\ell_f$ will vary from about 0.54 to 0.60.

Equation (4) results can be changed to body diameters by multiplying Eq. (4) by ℓ_f/d to obtain

$$(x_{\text{c.p.}}/\ell_f)(\ell_f/d) = (x_{\text{c.p.}})_f/d \tag{5}$$

The combination of Eqs. (2–5) gives the C_{N_α} and $x_{\text{c.p.}}$ for flares at all Mach numbers. C_N is simply

$$C_{N_f} = \left(C_{N_\alpha}\right)_f \alpha \tag{6}$$

for small AOA. Because most flare configurations are designed to fly at small AOA, Eqs. (5) and (6) determine two of the desired static aerodynamic terms for a flare. The pitching moment coefficient of the flare about some reference location is then

$$C_{M_f} = -[(x_{\text{c.p.}} - x_{\text{c.g.}})/d]C_{N_f} \tag{7}$$

Body Alone Pitch Damping Moment

The body alone dynamic derivatives are all computed based on an empirical model developed by Whyte,[14] called Spinner. The version that is incorporated into the AP98 is basically the same version as initially included in the APC series in 1977. The technology of Ref. 14 was based on curve fits of data using standard spin-stabilized rounds. The curve fits have key parameters of length, boattail length, and Mach number for the dynamic derivative predictions. Magnus force and moments are also estimated at both 1- and 5-deg AOA to incorporate some nonlinearity due to AOA in the Magnus moment. The databases on which the empirical curve fits were based were primarily limited to about 5.5 calibers and Mach numbers less than 5.0 (newer versions of Spinner may now be available that remove these limits). This upper length was because no spin-stabilized projectile is in current use that is longer than 5.5 calibers. However, length was considered in a linear sense for roll damping moment and one of the databases had length as a parameter for pitch damping moments as well.

Since the late 1960s and early 1970s, the U.S. Army Research Laboratory (ARL) at Aberdeen, Maryland, has developed a very good CFD capability to compute both static and dynamic derivatives of projectiles, with and without flares. References 7, 8, 10, and 11 are some of the reports generated by ARL using CFD. As a result of these many CFD computations, and comparison to data, one can now fine tune the older Spinner model[14] to be more representative of a broader class of configurations.

In comparing the AP98 (in essence the Spinner model) predictions of pitch damping moment to ballistic range data and CFD predictions of Refs. 7, 8, 10, and 11, it was seen that the empirical Spinner predictions did not do a very good job in predicting pitch damping moments above $M_\infty = 1.2$ (see Table 2 comment). The Spinner results appeared to be reasonable for $M_\infty \le 1.2$, but overpredicted $C_{M_q} + C_{M_{\dot\alpha}}$ as Mach number increased. The higher the Mach number, the worse the predictions became. On the other hand, the errors followed a fairly smooth pattern, allowing a correction to be derived based on CFD results from Refs. 7, 8, 10, and 11.

The modified pitch damping moment coefficient for bodies without a flare present is, therefore,

$$C_{M_q} + C_{M_{\dot\alpha}} = \left(C_{M_q} + C_{M_{\dot\alpha}}\right)_S F_1 \tag{8}$$

where $(C_{M_q} + C_{M_{\dot\alpha}})_S$ is the value obtained from the AP98,[1] which basically uses Ref. 14. F_1 is an empirical decay factor for Mach number derived using the AP98 and Refs. 7, 10, and 11. Here, F_1 is a function of Mach number and total length of the projectile and is defined by the following model:

For $\ell/d \le 5.0$,

$$F_1 = 1.0, \qquad M_\infty \le 1.2$$
$$F_1 = 0.0043M_\infty^2 - 0.151M_\infty + 1.175, \qquad 1.2 < M_\infty \le 5.0$$
$$F_1 = 0.53, \qquad M_\infty > 5.0 \tag{9}$$

For $\ell/d = 8$,

$$F_1 = 1.0, \qquad M_\infty \le 2.0$$
$$F_1 = 0.0031M_\infty^2 - 0.0884M + 1.164, \qquad 2.0 < M_\infty \le 5.0$$
$$F_1 = 0.8, \qquad M_\infty > 5.0 \tag{10}$$

For $5 < \ell/d < 8$,

$$F_1 = F_1(\ell/d = 5) - [(\ell/d - 5)/3]$$
$$[F_1(\ell/d = 5) - F_1(\ell/d = 8)] \tag{11}$$

For $\ell/d \ge 12$,

$$F_1 = 1.0, \qquad M_\infty \le 2.0$$
$$F_1 = 0.0011M_\infty^2 - 0.111M_\infty + 1.178, \qquad 2 < M_\infty \ge 5.0$$
$$F_1 = 0.9, \qquad M_\infty > 5.0 \tag{12}$$

For $8 < \ell/d < 12$,

$$F_1 = F_1(\ell/d = 8) - [(\ell/d - 8)/4]$$
$$[F_1(\ell/d = 8) - F_1(\ell/d = 12)] \tag{13}$$

Pitch Damping Moment of Bodies with Flares

A typical body configuration with a flare present is shown in Fig. 1. As already mentioned, the AP98 code does not calculate a value of additional pitch damping due to the presence of a flare. The approximate method used here to represent the flare is basically to use the Ref. 15 approach where

$$\left(C_{M_q} + C_{M_{\dot\alpha}}\right)_f = -2\left(C_{N_\alpha}\right)_f [(x_{\text{c.p.}} - x_{\text{c.g.}})/d]_f^2 \tag{14}$$

Equation (14) was used in Ref. 15 to approximate the pitch damping moment coefficient of a wing, but here the flare replaces the wing planform area. $(C_{N_\alpha})_f$ of Eq. (14) is defined by Eq. (2). In Eq. (14), $(x_{\text{c.p.}})_f/d$ is defined by Eqs. (4) and (5) and Fig. 2. Finally, because Eq. (2) already includes the approximate reference areas, Eq. (14) is appropriate as it stands. Equation (14) only includes that portion of the flare area external to the cylindrical part of the body [see Eq. (1)] because the body alone pitch damping moment discussed earlier already includes the cylindrical part of the afterbody.

Results and Discussion

Static Aerodynamics of Flared Configuration

In this part of the paper, we will show the comparison of the approximate methods to predict aerodynamics of flared configurations to both CFD and experimental results. Static aerodynamic predictions of flared configurations will be considered first. Unfortunately, the authors were only able to find data in the literature for Mach numbers of 2.0 and greater. Hence, the new inclusion into the APC of flare static aerodynamics for $M_\infty < 1.2$ cannot be validated at present. A CFD code could be used for this purpose, but funding would not permit the authors to undertake a CFD study. However, existing static aerodynamic predictions for low supersonic to hypersonic Mach numbers can be assessed. It is suspected that the reason for the lack of static aerodynamic data at low Mach numbers for flare-stabilized configurations is that the practical application of flare configurations is at high Mach number. The use of flares at high Mach numbers is also made more relevant because fins lose their effectiveness as stabilizing devices as Mach number increases, along with posing problems for leading-edge heating and ablation. On the other hand, flares are just as effective at high Mach number as at low Mach number in providing stability, although they give high drag compared to fins, particularly at low Mach number. Four

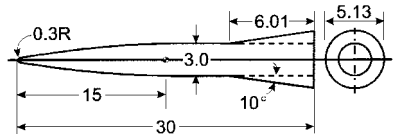

a) Body with 10-deg flare[16] (all dimensions in inches)

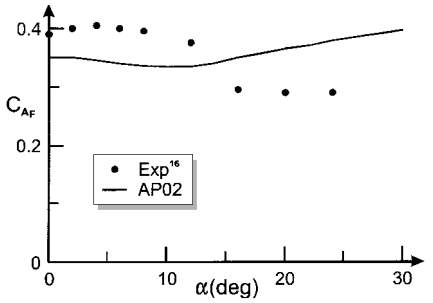

b) Forebody axial force coefficient

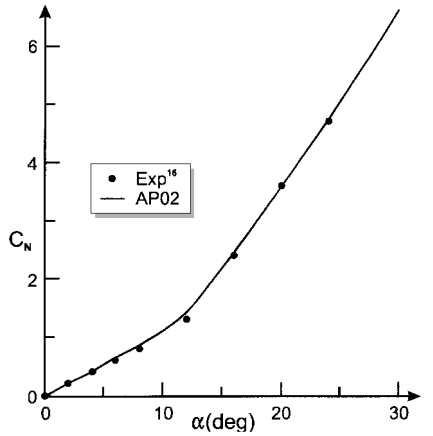

c) Normal force coefficient

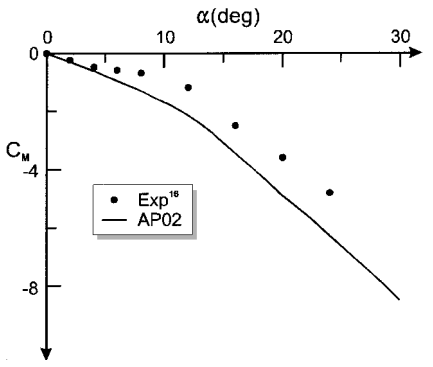

d) Pitching moment coefficient

Fig. 3 Comparison of theory and experiment for static aerodynamics of a body–flare configuration (M_∞ = 2.01 and R_N/ft = 2 × 10^6).

cases for static aerodynamics of flares are considered in Ref. 6. Only two of those cases will be presented here due to limited space.

The first case shown for static aerodynamics validation is given in Fig. 3 and is taken from Ref. 16. This configuration is a blunted von Kármán ogive–cylinder–flare case with a 10-deg, 2-caliber flare. Wind-tunnel data were taken at $M_\infty = 2.0$ and R_N/ft of 2×10^6 without a boundary-layer trip present. Comparison of the theory (here shown as AP02) to experiment for the forebody axial force, normal force, and pitching moment coefficients is given in Fig. 3. The axial force is not as accurate as desired. However, this inaccuracy could be because the base pressure term was subtracted from the total axial force. This term was larger than the friction and wave drag terms combined. Hence, a small error in measuring the base pressure of 5–10% could account for most or all of the discrepancy between theory and experiment for the axial force coefficient of Fig. 3b. Normal force predictions are excellent, and pitching moments are quite acceptable. The authors choose to place the accuracy criteria on c.p. vs pitching moment because pitching moment accuracy is dependent on the point about which the moments are taken. The average c.p. error is less than 4% of the body length, which means the predictions are within the ±4% of body length error accuracy goal stated for the AP02. The average normal force error is under 2%. Because no total axial force measurements were given, an accuracy assessment on the axial force cannot be given.

The second flared configuration where static aerodynamics is shown is given in Fig. 4. The Fig. 4 case is a very long (23.14-calibers) configuration with a flare that is 4.24 calibers in length and a flare angle that varies from 0 to 20 deg. Data were given in Ref. 17 at $M_\infty = 4.4$, 5.9, and 8.8. All three cases showed similar trends, and the AP02 predictions were similar, and so only

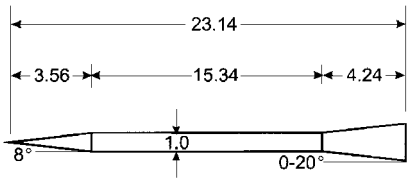

Schematic of F829 cone-cylinder-flare configuration[17] (all dimensions in calibers) (one caliber = 27.05 mm)

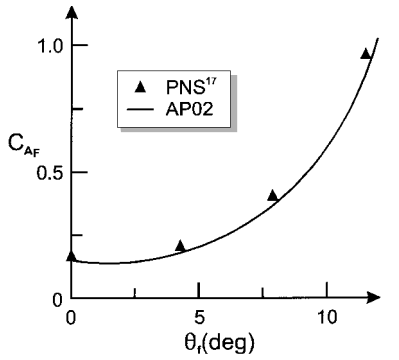

Forebody axial force coefficient

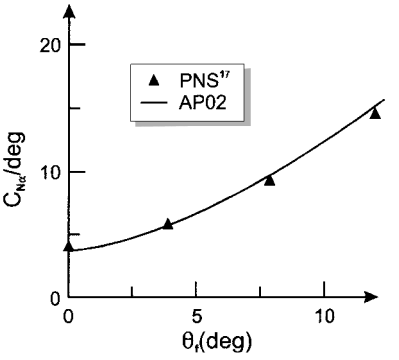

Normal force coefficient slope

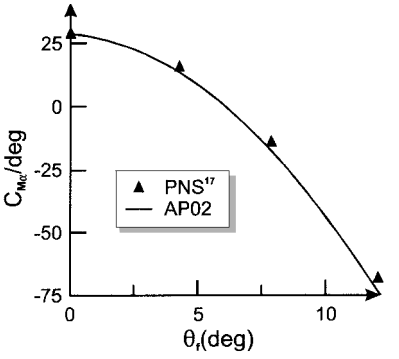

Pitching Moment Coefficient slope

Fig. 4 Static aerodynamics of F829 configuration (M_∞ = 5.9 and $\alpha \approx$ 0 deg).

the $M_\infty = 5.9$ case is shown in Fig. 4. Aerodynamics shown include the forebody axial force coefficient and the normal force and pitching moment slopes near $\alpha = 0$ deg. No experimental data were given in Ref. 4, only parabolized Navier–Stokes (PNS) calculations at sea-level conditions where fully turbulent flow was assumed. The AP02 predictions agree quite well with the PNS calculations for all of the aerodynamic coefficients at all flare angles.

Pitch Damping Moment of Body Alone Configurations

The next aerodynamic term to be considered in the validation process is body alone pitch damping moment where no flare is present. The modifications to the AP98 predictions (which are basically taken from the old General Electric Spinner program[14]) were discussed in the analysis section of this paper. A recent report from the ARL (Ref. 10) showed PNS calculations of pitch damping on a 5-, 6-, and 7-caliber secant–ogive–cylinder–boattail (SOCBT) and secant–ogive–cylinder (SOC). Computations were available from $M_\infty = 2$ to 5. These results were instrumental in the authors concluding that the AP98 pitch damping computations for a body alone needed improvement for higher Mach numbers. Although it is true that the CFD results can be in error, the results showed enough agreement with ballistic range data to convince the authors that the results from the AP98 were in error. Also note that, typically, ballistic range data can have scatter of up to 25% or more. CFD results will generally have a smooth and consistent trend as well, making it easier to develop an empirical model with CFD than with ballistic range data. Figure 5 shows the comparison of the improvements in the AP02 compared to the AP98 predictions and PNS predictions for pitch damping moment for a body alone (no flare present). Although the AP02 does not agree perfectly with the PNS computations, it shows drastic improvement over the AP98 for $M_\infty \geq 2.0$ at all of the body lengths (5, 6, and 7 calibers) shown in Fig. 5. The c.g. was held to a constant percent of the total body length of 60% in these calculations. A note of caution is given here to the reader. The Ref. 9 (and all ARL results) use a nondimensionalization of qd/V_∞ for the pitch damping whereas the NSWCDD uses $qd/(2V_\infty)$. Hence, all ARL results had to be multiplied by two to compare to NSWCDD results. Results for the SOCBT case were even better than those for the SOC case. These results are shown in Ref. 6.

The last body alone case considered for validation of the improved pitch damping predictions is given in Fig. 6. This configuration is the ARL–NSWCDD Spinner case, which consists of a 2.0-caliber tangent ogive nose followed by a 3-, 5-, and 7-caliber cylindrical afterbody. Total body lengths are, therefore, 5, 7, and 9 calibers. Results were given in Refs. 10 and 11 consisting of PNS calculations and ballistic range data. Data were available for all configurations for M_∞ between 1.3 and 2.5 and for the 7-caliber case, for M_∞ between 0.8 and 2.5. Also, several c.g. locations were given in Refs. 10 and 11, but only the case where the c.g. was at about the 60% location (which is typical of most ammunition) is shown here. Note that for Mach numbers below about 1.5, the old AP98 predicts pitch damping quite adequately. Also, for Mach numbers as high as 2.5, predictions are within 10% of both data and CFD calculations for the AP98, and so only minor improvements are shown using the AP02 for this configuration due to the low Mach numbers considered. This makes sense because the Ref. 14 methodology was based on available data, which in the 1970s consisted mainly of shells with $0.8 \leq M_\infty \leq 2.5$ and lengths of 4–7 calibers. The second point to note from Fig. 6 is that for the longest configuration ($\ell = 9$ calibers), there is a large scatter in the ballistic range data, but the predictions still appear to be reasonable, given the large scatter in data. As already mentioned, it is not unusual to have a scatter of 25% or more in ballistic range data for the pitch damping moment coefficient.

Pitch Damping of Flared Configurations

We are now ready to validate the AP02 predictions of pitch damping moment for flare configurations. Recall that the methodology for pitch damping moments of flares was the primary reason for this paper and the improvements to the AP98 because the AP98 did not give any additional pitch damping due to the presence of a flare. Figure 7 gives the first case considered, which is termed the CS-V4-1 configuration in Ref. 8. This configuration consists of a blunt cone–cylinder–flare, where the flare angle is 6 deg and the flare length is 3.51 calibers. The overall configuration length is 15.36 calibers. The configuration of Fig. 7 shows rifling grooves, but a smooth body was assumed in the PNS and aeroprediction calculations. Pitch damping results are shown in Fig. 7 for Mach numbers 0.4–5.0 from the AP02 and AP98. PNS results are shown from $M_\infty = 3$ to 4.5, and ballistic range results are shown at $M_\infty = 4.0$. Note that the AP02 methodology agrees much more closely to the experimental data and PNS results than does the AP98. The AP98 results are basically those of a cone–cylinder that is 15.36 calibers long.

Figure 8 shows pitch damping results for a configuration similar to that of Fig. 7, except that the flare is longer, 4.49 vs 3.51

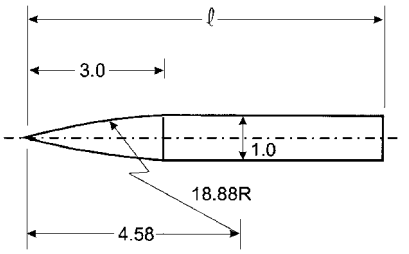

Schematic of the SOC configuration[9] (all dimensions in calibers) (one caliber = 57.2 mm)

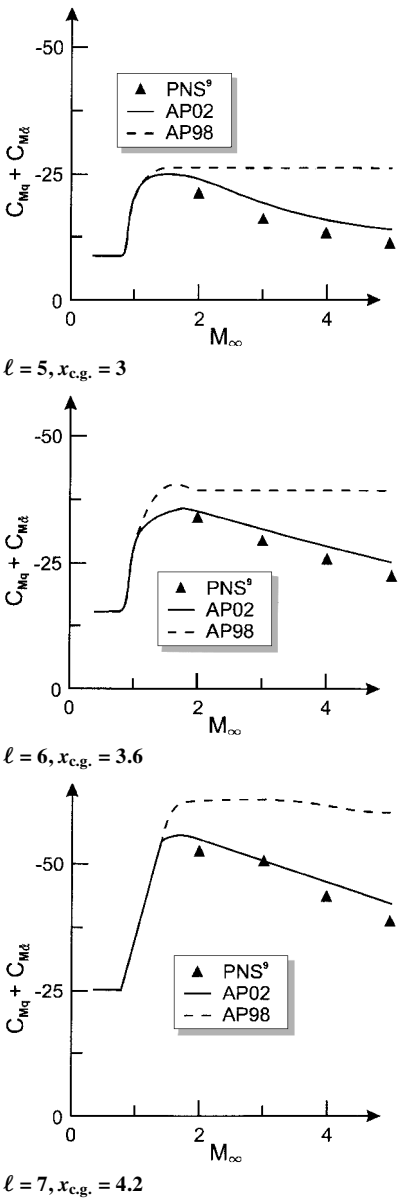

Fig. 5 Pitch damping moment coefficient predictions for the SOC configuration.

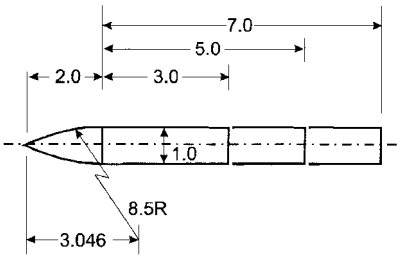

Schematic of the ANSR[10] (all dimensions in calibers) (one caliber = 20 mm)

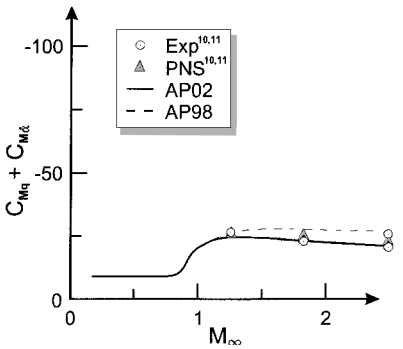

$\ell = 5, x_{c.g.} = 3$

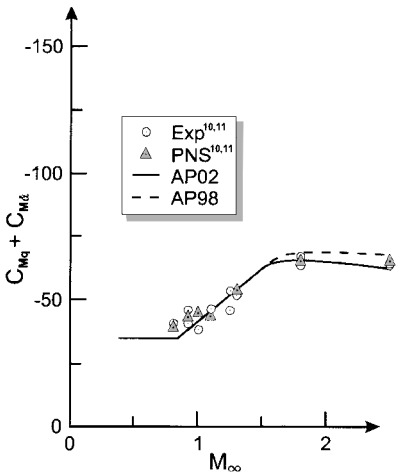

$\ell = 7, x_{c.g.} = 4.0$

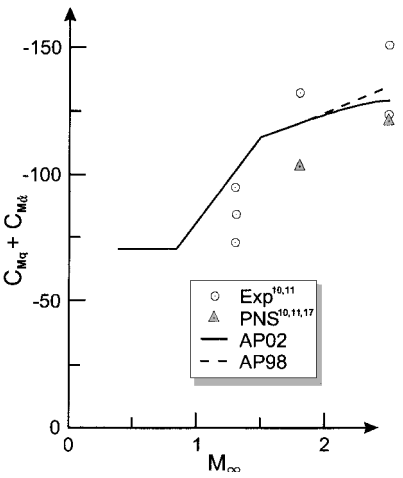

$\ell = 9, x_{c.g.} = 5.0$

Fig. 6 Pitch damping moment coefficient predictions compared to experiment for ANSR.

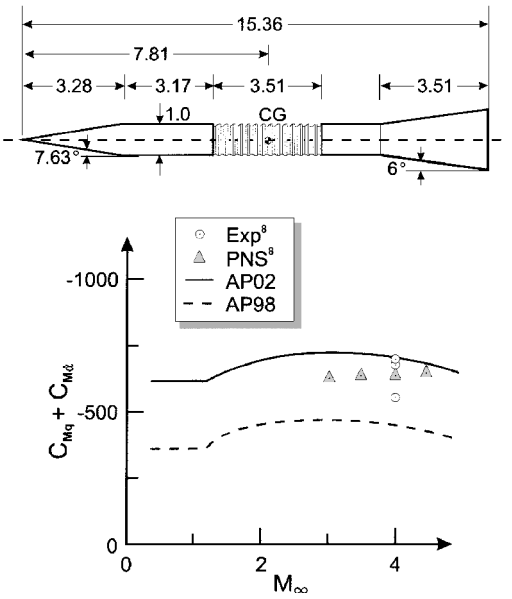

Fig. 7 Comparison of theory and experiment for pitch damping moment coefficient of CS-V4-1 configuration. CS-V4-1 flare stabilized projectile geometry[8] (all dimensions in calibers) (one caliber = 8.28 mm).

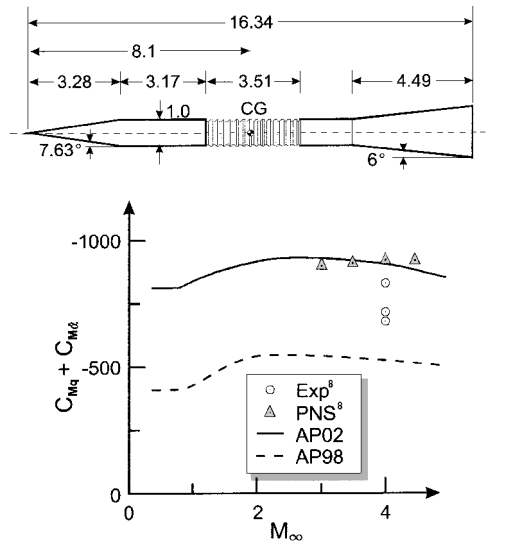

Fig. 8 Comparison of theory and experiment for pitch damping moment coefficient of CS-V4-2 configuration. CS-V4-2 flare stabilized projectile geometry[8] (all dimensions in calibers) (one caliber = 8.28 mm).

calibers, and the overall Fig. 8 configuration length is longer (16.34 vs 15.36 calibers) than that of Fig. 7. Again, AP98 and AP02 results are shown for Mach numbers of 0.4–5, whereas PNS calculations were available for Mach numbers of 3–4.5, and ballistic range data were available for $M_\infty = 4.0$ only. The AP02 results match the PNS calculations quite nicely, with the AP98 being much lower than the PNS results due to not accounting for the flare. The ballistic range data are somewhat lower than the PNS data and AP02 for this configuration, possibly due to the impact of the grooves on the pitch damping. Also, the ballistic range data show scatter in the data, which is typical of dynamic derivatives.

The third case considered for pitch damping is the CAN4 (Ref. 18) projectile. The pitch damping results are shown in Fig. 9 in terms of AP98 and AP02 for Mach numbers 2–6 and CFD and ballistic range results at $M_\infty = 4.4$ and 5.72. The AP02 results agree very well with the CFD results, and both are 10–15% lower than the experimental data. Errors of ±20% are quite reasonable, and so these results are quite acceptable for dynamic derivative predictions. However, the older AP98 gives unacceptable results.

The fourth flared configuration where experimental pitch damping data or CFD computations was found in the literature is shown

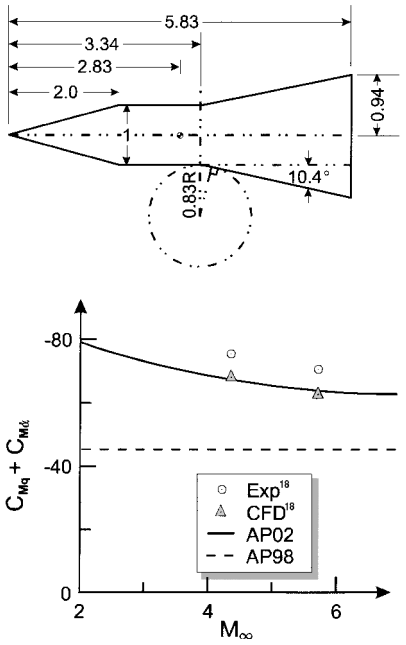

Fig. 9 Comparison of theory and experiment for pitch damping moment coefficient of CAN4 projectile. CAN4[18] projectile schematic (all dimensions in calibers).

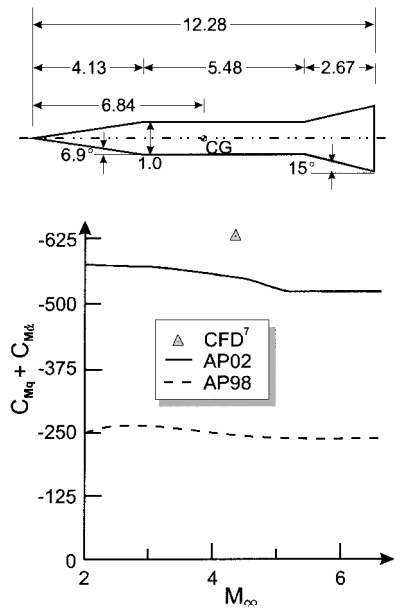

Fig. 10 Comparison of theory and experiment for pitch damping moment coefficient of flared projectile configuration. Flared projectile configuration[7] (all dimensions in calibers).

in Fig. 10 (Ref. 7). This configuration is also a cone–cylinder–flare of 12.28 calibers total length. It has a flare with a 15-deg flare angle that is 2.67 calibers in length. Only one CFD data point was given in Ref. 7 at $M_\infty = 4.4$. However, AP02 and AP98 computations are shown for Mach numbers of 2–6.0. The AP02 results are about 12% lower than the data point at $M_\infty = 4.4$ ($C_{M_q} + C_{M_{\dot{\alpha}}} = -550$ vs -625), which is considered to be acceptable prediction accuracy. However, the AP98 predictions are about 60% too low.

The final configuration where CFD or experimental pitch damping data was found was also taken from Ref. 7, and results are given in Fig. 11. It consists of a 13.16-caliber cone–cylinder–flare where the flare angle varies from 4 to 14 deg. Again, only $M_\infty = 4.4$ data were given in Ref. 7. Notice the good agreement of the AP02 to the CFD computations. Here, the worst error of the AP02 compared to the CFD is under 6% for the $\theta_f = 14$ deg case. Again, the AP98 gives unacceptable agreement to the CFD, except for small θ_f.

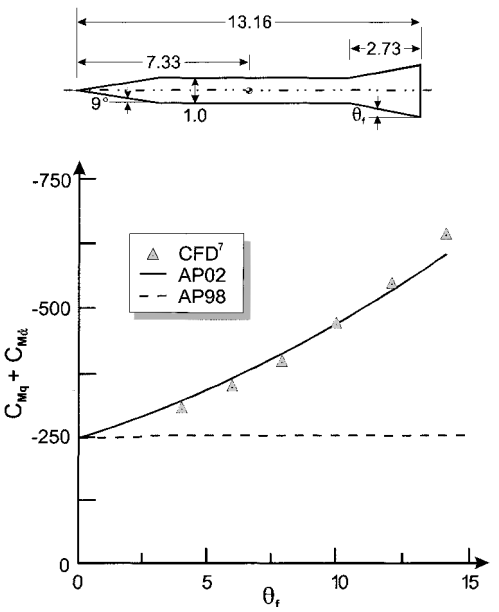

Fig. 11 Comparison of three theoretical predictions of pitch damping moment coefficient for various flare angles ($M_\infty = 4.4$). Control projectile configuration[7] (all dimensions in calibers).

Conclusions

To summarize, new capability has been added to the NSWCDD APC to allow static aerodynamics to be computed for flared configurations at all Mach numbers. Improvements have been added to pitch damping predictions for high Mach numbers for body alone configurations (no flare present). Finally, new capability has been added to allow pitch damping computations to be made for flare configurations for all Mach numbers where the APC is operational (Mach numbers 0–20).

In comparing the new aeroprediction code (AP02) to experimental data and both parabolized and full Navier–Stokes predictions, the following conclusions were drawn:

1) Comparison of static aerodynamic predictions for configurations that have flares to experimental data and CFD computations appears to show that the AP98 and AP02 give predictions within the standard accuracy goals for configurations with wings or tails. That is average accuracy of ±10% for axial and normal force and ±4% of the body length for c.p.

2) Comparison of AP02 pitch damping predictions for bodies without flares to the AP98, experimental data, and CFD computations showed the AP02 predictions to be superior to the AP98 for $M_\infty > 2$ for all cases considered. The average accuracy goal of ±20% was met for the AP02 but not with the AP98.

3) Comparison of the AP02 pitch damping predictions for bodies with flares to the AP98, experimental data, and CFD computations showed the AP02 predictions to be within the desired average accuracy goal of ±20%. However, the AP98 could be off as much as 60–70% due to failure to account for the flare.

4) No data (either static or dynamic) were found for flared configurations for Mach numbers below 2.0. Hence, the new capability for both static aerodynamics for $M_\infty < 1.2$ and pitch damping for flared configurations could not be adequately validated for low Mach numbers. Although the authors would like to have data for validation in this Mach number range, it may be impractical from a usage standpoint. This impracticality is driven by the fins being better at both stability and drag for moderate to lower supersonic Mach numbers than flares.

5) Although the pitch damping methods for flared configurations have not been validated for Mach numbers below 2.0, the authors believe they can still be used with confidence in preliminary design tradeoffs to compare flared configurations to those with wings. This belief is due to the accuracy of the methodology for Mach numbers above 2.0 and the consistency of the methodology for Mach numbers above and below 2.0.

References

[1]Moore, F. G., McInville, R. M., and Hymer, T., "The 1998 Version of the NSWC Aeroprediction Code: Part I—Summary of New Theoretical Methodology," U.S. Naval Surface Warfare Center, Dahlgren Div., Rept. NSWCDD/TR-98/1, Dahlgren, VA, April 1998.

[2]Moore, F. G., *Approximate Methods for Weapon Aerodynamics*, edited by P. Zarchan, Vol. 186, Progress in Astronautics and Aeronautics, AIAA, Reston, VA, 2000.

[3]Moore, F. G., McInville, R. M., and Robinson, D. I., "A Simplified Method for Predicting Aerodynamics of Multi-Fin Weapons," U.S. Naval Surface Warfare Center, Dahlgren Div., Rept. NSWCDD/TR-99/19, Dahlgren, VA, March 1999.

[4]Moore, F. G., and McInville, R. M., "Refinements in the Aeroprediction Code Based on Recent Wind Tunnel Data," U.S. Naval Surface Warfare Center, Dahlgren Div., Rept. NSWCDD/TR-99/116, Dahlgren, VA, Dec. 1999.

[5]Hymer, T. C., Downs, C., and Moore, F. G., "Users Guide for an Interactive Personal Computer Interface for the 1998 Aeroprediction Code (AP98)," U.S. Naval Surface Warfare Center, Dahlgren Div., Rept. NSWCDD/TR-98/7, Dahlgren, VA, June 1998.

[6]Moore, F. G., and Hymer, T. C., "Improvements in Pitch Damping for the Aeroprediction Code with Particular Emphasis on Flare Configurations," U.S. Naval Surface Warfare Center, Dahlgren Div., Rept. NSWCDD/TR-00/009, Dahlgren, VA, April 2000.

[7]Sturek, W. B., Nietubicz, C. J., Sahu, J., and Weinacht, P., "Recent Applications of CFD to the Aerodynamics of Army Projectiles," U.S. Army Research Lab., Rept. ARL-TR-22, Aberdeen Proving Ground, MD, Dec. 1992.

[8]Weinacht, P., "Navier–Stokes Predictions of Pitch-Damping for a Family of Flared Projectiles," U.S. Army Research Lab., Rept. ARL-TR-591, Aberdeen Proving Ground, MD, Oct. 1994.

[9]Qin, N., Ludlow, D. K., Shaw, S. T., Edwards, J. A., and Dupuis, A., "Calculation of Pitch Damping Coefficients for Projectiles," AIAA Paper 97-0405, Jan. 1997.

[10]Weinacht, P., Sturek, W. B., and Schiff, L. B., Navier–Stokes Predictions of Pitch-Damping for Axisymmetric Shell Using Steady Coming Motion," U.S. Army Research Lab., Rept. ARL-TR-575, Aberdeen Proving Ground, MD, Sept. 1994.

[11]Weinacht, P., "Prediction of Pitch Damping of Projectiles at Low Supersonic and Transonic Velocities," AIAA Paper 98-0395, Jan. 1998.

[12]Wu, J. M., and Aoyoma, K., "Transonic Flow-Field Calculation Around Ogive Cylinders by Nonlinear–Linear Stretching Method," U.S. Army Missile Command, TR RD-TR-70-12, April 1970; also AIAA Paper 70-189, Jan. 1970.

[13]"Equations, Tables, and Charts for Compressible Flow," NACA Rept. 1135, 1953.

[14]Whyte, R. H., "Spinner—A Computer Program for Predicting the Aerodynamic Coefficients of Spin Stabilized Projectiles," General Electric Class 2 Repts., 1969.

[15]Chin, S. S., *Missile Configuration Design*, McGraw–Hill, New York, 1961, pp. 134–138.

[16]Robinson, R., "Wind Tunnel Investigation at a Mach Number of 2.01 of the Aerodynamic Characteristics in Combined Angles of Attack and Sideslip of Several Hypersonic Missile Configurations with Various Canard Controls," NACA RM L58A21, March 1958.

[17]Guidos, B. J., "Static Aerodynamics CFD Analysis for 120-mm Hypersonic KE Projectile Design," U.S. Army Research Lab., Rept. ARL-MR-184, Aberdeen Proving Ground, MD, Sept. 1994.

[18]Dupuis, A., and Edwards, J. A., "Analysis of Free-Flight Data for the CAN4 Hypersonic Research Projectile," AIAA Paper 98-0581, Jan. 1998.

M. S. Miller
Associate Editor